

SIGNATURE OF DARK MATTER AT THE CENTER OF MILKY WAY

A REPORT

*submitted in partial fulfillment of the requirements
for the award of the dual degree of*

Bachelor of Science-Master of Science

in

PHYSICS

by

AVISHEK SINGH

(12030)



**DEPARTMENT OF PHYSICS
INDIAN INSTITUTE OF SCIENCE EDUCATION AND
RESEARCH BHOPAL
BHOPAL - 462066**

April 2017



भारतीय विज्ञान शिक्षा एवं अनुसंधान संस्थान भोपाल
Indian Institute of Science Education and Research Bhopal
(Estb. by Ministry of HRD, Govt. of India)

Certificate

This is to certify that **AVISHEK SINGH**, BS-MS (Physics), has worked on the project entitled '**SIGNATURE OF DARK MATTER AT THE CENTER OF MILKY WAY**' under my supervision and guidance. The content of this report is original and has not been submitted elsewhere for the award of any academic or professional degree.

April 2017
IISER Bhopal

Dr. Rajib Saha

Committee Member

Signature

Date

ACADEMIC INTEGRITY AND COPYRIGHT DISCLAIMER

I hereby declare that this project is my own work and, to the best of my knowledge, it contains no materials previously published or written by another person, or substantial proportions of material which have been accepted for the award of any other degree or diploma at IISER Bhopal or any other educational institution, except where due acknowledgement is made in the document.

I certify that all copyrighted material incorporated into this document is in compliance with the Indian Copyright Act (1957) and that I have received written permission from the copyright owners for my use of their work, which is beyond the scope of the law. I agree to indemnify and save harmless IISER Bhopal from any and all claims that may be asserted or that may arise from any copyright violation.

**April 2017
IISER Bhopal**

AVISHEK SINGH

ACKNOWLEDGMENT

First and foremost I offer my sincerest gratitude to my supervisor, Dr Rajib Saha, who has supported me throughout my thesis with his patience and knowledge whilst allowing me the room to work in my own way. I attribute the level of my Masters degree to his encouragement and effort and without him this thesis, too, would not have been completed or written. One simply could not wish for a better or friendlier supervisor. I am very grateful to the department of Physics at Indian Institute of Science Education and Research Bhopal for providing me a platform to conduct this research.

Beyond Physics (which sometimes seemed to be nothing more than a distant dream) Hare Krishna, Shubham Singh and Arpit Kumar has been a companionable group-mates for two years as well as colleagues. Also I would like to thank my friends Amit Singh, Prince Kumar Maurya for support and encouragement throughout my master's studies.

Finally, I must express my very profound gratitude to my parents for providing me with unfailing support and continuous encouragement throughout my years of study and through the process of researching and writing this thesis. This accomplishment would not have been possible without them. Thank you.

Special thanks to the Department of Science and Technology, Government of India for providing the necessary funds throughout the stay at Indian Institute of Science Education and Research Bhopal.

AVISHEK SINGH

ABSTRACT

In this report, we implemented Iterative Linear Combination (ILC) of WMAP maps in modified way and Metropolis-Hasting technique of Markov Chain Monte Carlo simulation to find the “Haze/Bubble” signals at microwave wavelength in the center of our galaxy (Milky Way) from WMAP data and also to estimate the correct spectral index for “Haze” signals & synchrotron signals. The Haze is a distinct component of diffuse galactic emission, centered on the Galactic center and extends from 35° to 50° in Galactic latitude and from 15° to 20° in longitude.

By using *Wilkinson Microwave Anisotropy Probe (WMAP)*[1], we are able to filter these “Haze” signals and able to provide correct spectral index for these “Haze” signals. The modified *Iterative linear Combination (ILC)* of WMAP provided spectral index of these “Haze” signals, $\beta_{DM} = -2.56 \pm 0.01$ and *Metropolis-Hasting* technique of *Markov Chain Monte Carlo (MCMC)* simulation provided spectral index of these “Haze” signals, $\beta_{DM} = -2.52 \pm 0.01$, which matches with the spectral index reported in many papers. As accompanying results of the method we also reconstructed *Synchrotron Emission* maps and estimated spectral index. only *Iterative linear Combination (ILC)* provided “synchrotron” spectral index, $\beta_s = -3.10 \pm 0.01$ and the implementation of *Metropolis-Hasting* technique of *Markov Chain Monte Carlo (MCMC)* simulation provided “synchrotron” spectral index, $\beta_s = -2.90 \pm 0.01$. The *Metropolis-Hasting* technique of *Markov Chain Monte Carlo (MCMC)* simulation as implemented in this work has interesting property that it can sample as many parameters as you want. We argue that, our method of “Haze” signal detection and spectral index determination is a maximum likelihood method.

CONTENTS

Academic Integrity and Copyright Disclaimer	ii
Acknowledgment	iii
Abstract	iv
1. Introduction	1
2. Component Description	3
2.1 What is Dark Matter?	3
2.2 Foregrounds	5
2.2.1 Synchrotron Emission	6
2.2.2 Free-Free Emission	7
2.2.3 Thermal Dust Emission	8
2.2.4 Spinning Dust Emission	9
2.2.5 CO Molecular Cloud Emission	10
2.3 Cosmic Microwave Background(CMB)	10
3. Description of Data	12
3.1 WMAP Data And Templates	12
3.2 Smoothing of maps	14
3.3 Mask	16
4. Analysis of Data	17
4.1 Calculation of power spectrum and Weights	17
4.1.1 Cross-power spectrum estimation	17
4.1.2 Estimation of weights for cleaned maps	18

4.2	Noise Estimation	20
4.3	χ^2 Calculation	24
5.	Methodology	25
5.1	Simple Subtraction Technique	25
5.1.1	Only CMB is removed	25
5.1.2	CMB and monopoles are removed	26
5.1.3	CMB, monopoles and free-free are removed	27
5.2	Use of Markov Chain Monte Carlo Approach to Enhance Results	27
5.2.1	Markov Chain Monte Carlo Approach	28
5.2.2	Sampling of Dipoles	29
5.2.3	Sampling of Spectral Indices and Monopoles	30
6.	Results	31
6.1	Only CMB is subtracted	31
6.2	CMB and Monopoles are subtracted	33
6.3	CMB, Monopoles and Thermal Dust are subtracted	35
6.4	Results using Markov Chain Monte carlo Approach	36
7.	Summary	39

1. INTRODUCTION

After the Wilkinson Microwave Anisotropy Probe (WMAP) released data, It changed our understanding of cosmology[1] and physical process of our galaxy's interstellar medium[2]. from this data some expected processes like thermal dust emission, synchrotron emission, free-free emission from electron-ion scattering, spinning dust emission (anomalous microwave emission)[3] and CO molecular emission. But we also get something the most mysterious one was "Haze"[4] emission discovered by Finkbeiner which was found in the galactic center and it was appeared almost spherically symmetric. It's intensity decreases as we move away from galactic center and it's origin was to found. Initially Fikbeiner et al. in 2004[4] characterized this Haze signal as free-free emission because of its hard spectrum[4] but at that time the significant systematic uncertainty in the measured spectrum was not appreciated.

After the analysis by Dobler & Finkbeiner (2008a)[5] of WMAP three year data, the key to determine the origin of Haze, systematic uncertainty in the determination of the Haze spectrum was identified. This uncertainty was due to residual foreground contaminating the CMB radiation and this generates the consequences of chance morphological correlations between the Haze and Cosmic Microwave Background Radiation. The spectrum of Haze was found to be harder than synchrotron emission and softer than free-free emission as compare to elsewhere in the galaxy. Later on it was noticed that elimination of this systematic uncertainty is possible by using Plank mission data, which produce less foreground contaminated Cosmic Microwave Background (CMB) radiation signals.

After the discovery of gamma-ray counterpart by Dobler et al.[6] of this emission by using Fermi Gamma-ray Space Telescope, the synchrotron nature

of haze was supported. The observations made by Fermi Gamma-ray Space Telescope were consistent with inverse Compton signal which was generated by electrons with same amplitude and spectrum as WMAP's microwave Haze yields. Further in Su et al. (2010)[7] work it appeared that Fermi haze have sharp edges and then it was named as "Fermi Bubbles". Now there has been many theoretical interest in determining the origin of this hard spectrum of haze. Many astrophysicist and cosmologist came up with their suggestions like Galactic wind (Crocker & Aharonaian 2011)[8], enhanced supernova rates (Biermann et al (2010)[9], and co-annihilation of dark matter particles in the galactic center (Hooper et al 2007)[10]. All above scenarios can reproduce some properties of haze by no one can completely match all the observed characteristics.

After many observational evidences , there are may many suggestions that this microwave haze is either not synchrotron emission (Gold et al. 2011)[11] or artifact of analysis procedure (Mertsch & Sarkar 2010)[12]. Initial the second solution was supported by some alternative analysis of WMAP data which found no evidence of Haze (Eriksen et al. 2006)[13] but more recently Pietrobon in 2012 showed that all the above analysis can not separate the haze emission from low frequency combination of free-free, spinning dust and soft synchrotron. Later on in 2013 by using Plank mission data plank collaboration[14] provided the evidence of existence of haze signal by independent experiment. They not only separated haze signals but also eliminated the uncertainty in the spectrum which was hindered observational and theoretical studies for nearly a decades

Now in this project we will revisit the galactic center in search of this mysterious galactic haze/bubble with combination of WMAP and Plank mission data. The combination of WMAP and Plank mission data will give much accurate and clear haze signal. In this report I will discuss about components in chapter 2, we will describe about data that we used in our project in chapter 3 then in chapter 4 and 5 we will discuss about methodology and theory behind analysis of data and in last part of this report in chapter 6 and 7 we will publish our results and summarize our work with future plans.

2. COMPONENT DESCRIPTION

In this chapter in section 2.1 we will discuss about evidences of dark matter detection, in section 2.2 We will discuss about all kinds of foreground emissions which we need to remove from WMAP maps and in 2.3 we will discuss about Cosmic Microwave Background (CMB) radiation.

2.1 What is Dark Matter?

Photons brings almost all information from celestial bodies. We see objects because they emit light, and in some other cases like nebulae, we notice dark regions against luminous background which are due to absorption of light. Thus light absorption and light emission allows us to trace the matter in the universe. Photon emission from astronomical bodies are detected by modern instruments in radio, infrared, X-ray and gamma ray band. According to present data astronomical bodies of different nature emit or absorb photons in very different ways. some bodies emit more light on other hand some emit less light per mass unit. emissivity of the body can be described by the mass-to-light ratio of object. Thus we can say that mass-to-light ratio M/L varies in very large range. Thus natural question arises: Do all astronomical bodies emit or absorb light? And the observations done in past centuries clearly tell us that answer is probably NO.

Generally astronomers measure mass by object emission but mass of astronomical bodies can also be determined by the motion of other bodies around or within the body. In many cases the total mass calculated by this way exceeds the total luminous mass of all known astronomical bodies, and this hypothetical matter is called Dark Matter.

In last ten years the picture of dark matter[15] has become much clear. Dark matter evidence is summarized in a beautiful 1988 review article by Virginia Trimble. I will recall few important elements here.

In 1933, Fritz Zwicky measured the mass of Coma cluster of galaxies. He measured the relative velocities of the galaxies using their Doppler shift. he computed the mass using virial theorem on the gravitational potential, and he found the mass which was times the mass of visible stars and galaxies in the cluster.

Again astronomers systematically measured the rotational velocity profile (rotation curves) for many galaxies in 1970's. They expected that the mass of the galaxy is concentrated in the star visible region and outside this region velocities will fall off as $1/\sqrt{r}$. but the analysis shows that velocities are constant. According to Rubin, Thonnard, and Ford, in NGC 3067 galaxy, rotation velocity profile maintain large value at a distance of 40 kpc (120,000 light-years) from the center of galaxy. From the measurements it is found the rotation curve of our galaxy is also flat up to 100 kpc distance from center.

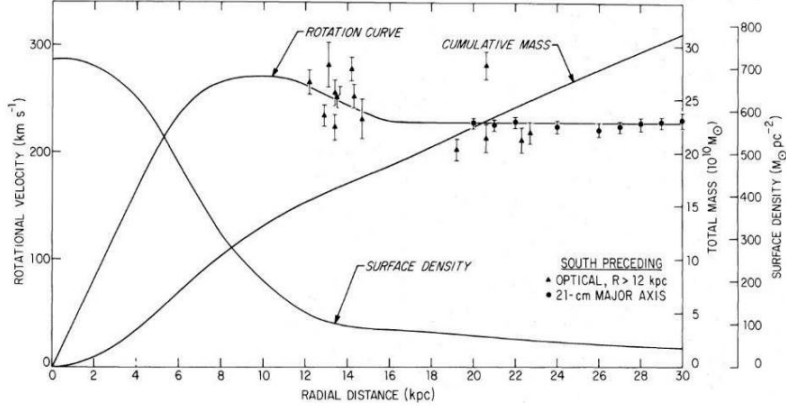


Fig. 2.1: Graph for galaxy rotation curve of orbital velocity with respect to radial distance from the center of galaxy. Source: arxiv:0901.0632[15]

Above picture is a galaxy rotation curve of M31 by roberts & Whitehurst(1975). The filled triangles shows the optical data from Rubin & Ford(1970).

In last few decades cosmologists have worked on the way of indirect detection of dark matter, which is related to dark matter annihilation. In search of dark matter astronomers used NASA's Fermi Gamma-ray telescope

to map galaxy. They tried to account for all known light sources in the maps and removed signals from gas and dust, light from stars and every object that might emit radiation, then they get a tiny excess of gamma radiation. Then they concluded that this signal might be due to annihilation of dark matter at the center of galaxy. Again it is not very clear that this is really a dark matter signal or something else. because the center of galactic plane is very tricky place. There are many gamma ray sources that might be mimicking a dark matter signal as well as yet another undiscovered phenomena that might account for the radiation.

2.2 Foregrounds

Cosmic Microwave Background (CMB) anisotropies[16] are most powerful probe of the cosmology among all cosmological observations. Strong constraints on cosmological parameters are already made by Experiments performed through satellites like COBE[17], WMAP[18], Planck[19] and these constraints are mainly derived from the total intensity anisotropies. Due to Thomson scattering at the recombination epochs, CMB photons are polarized at $\leq 10\%$. Through ongoing experiments, the detection of B mode polarization has provided a strong evidence of primordial gravitational waves, because B-mode polarization can not be generated by scalar density mode. All such information will be available only if the source contaminating CMB are removed. Most part of cosmological information comes from large angular scale of CMB anisotropies and the main source of uncertainty is the contamination by foreground emission from the galaxy. Now it is well known which that synchrotron emission from the galaxy dominates at low microwave frequencies and the thermal dust dominates at higher frequencies. In mid range frequencies free-free emission is dominating.

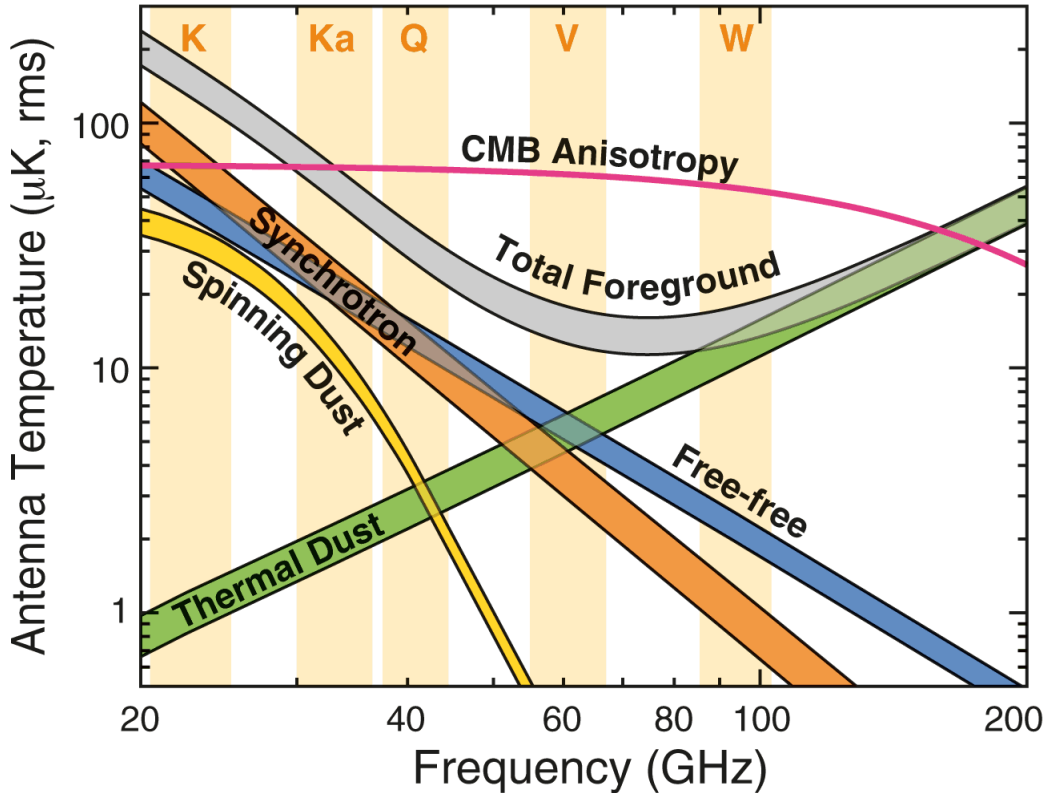


Fig. 2.2: Plot for the foreground component emission with frequency range[20]. Source: ApJS, vol. 208, issue 2, id. 20, 54 pp.(2013)

2.2.1 Synchrotron Emission

The main source of synchrotron emission is interaction between cosmic ray electrons and magnetic field in the galaxy. The intensity of the emission depends on the strength of magnetic field and cosmic ray energy, and therefore there is a significant spatial variations on the sky. For electrons power-law energy distribution $N(E) \propto E^{-p}$, the spectrum of synchrotron emission becomes $T_\nu \propto B^{(p+1)/2} \nu^\beta$ with $\beta = -(p + 3)/2$. Generally the value of β is $\beta \approx -2.5$ at radio frequency and steeper values $\beta \approx -3.0$ at 10 GHz frequency, with variations of ± 0.2 . Cosmic ray's aging effect defines the steeping and flattening is defined by superposition of multiple components. The spatial variation and uncertainty in the spectral index and the possibility of steepening and/or flattening of the spectrum are the

key issues for foreground modeling and component separation. Synchrotron emission is dominating in lower frequency range.

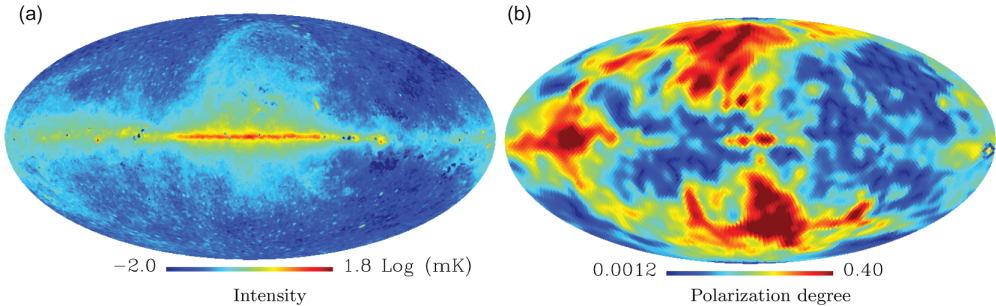


Fig. 2.3: (left) Synchrotron emission at 23 GHz in $\log_{10}(\text{mK})$ estimated in WMAP nine-year analysis using Maximum Entropy method. (Right) Polarization degree at 5° resolution. The intensity and the polarization data is based on MCMC model from the WMAP nine-year data[21].

Synchrotron photons are polarized perpendicular to the field lines because they are emitted by cosmic ray electrons accelerated by magnetic fields.

2.2.2 Free-Free Emission

Thermal bremsstrahlung is another name of free-free emission. Free-free emission arises due to electron-ion scattering in interstellar plasma. This emission can be traced by H_{α} line emission, both of which come dominantly from H_{II} region in the galaxy.

The intensity of free-free emission can be calculated by an integration along the line of sight as $I_{\nu} = \int j_{\nu} ds$, for optically thin plasma.

where,

$$j_{\nu} = 5.4 \times 10^{-16} \frac{g_{ff} Z_i^2 n_e n_i}{\sqrt{T_e}} \exp\left(-\frac{h\nu}{kT_e}\right) \text{ Jy sr}^{-1} \text{ cm}^{-1} \quad (2.1)$$

Here, n_e and n_i represents number densities of electron and ion, Z_i is atomic number and $T_e \approx 8000k$ is electron temperature. g_{ff} is gaunt factor of free free emission is given by,

$$g_{ff} = \frac{\sqrt{3}}{\pi} \left[\ln \frac{(2\pi kT)^{\frac{3}{2}}}{\pi e \nu \sqrt{m_e}} - \frac{5\gamma}{2} \right] \quad \text{for } h\nu \ll kT \quad (2.2)$$

where e is electron charge, m_e is electron mass, and γ is the Euler constant.

Observed intensity I_ν can also be expressed terms of brightness temperature T_B and fluctuation in thermodynamic temperature ΔT_{CMB} .

$$\Delta T_{CMB} = \frac{(e^x - 1)^2}{x^2 e^x} T_B = \frac{(e^x - 1)^2}{x^2 e^x} \frac{\lambda^2}{2k} I_\nu \quad (2.3)$$

where $x = \frac{h\nu}{kT_{CMB}}$ and $T_{CMB} = 2.725K$. Here we quote the WMAP K-band value that $T_B \propto \nu^{-2.14}$ for $T_e \approx 8000k$.

The scattering direction of electrons are isotropic and random therefore thermal free-free emission is intrinsically polarized. Though magnetic field can break the isotropic but the interstellar magnetic field is not strong enough to generate polarization at microwave frequency. So free-free emission is found polarized with an upper limit of 3.4% at the 95% confidence level.

2.2.3 Thermal Dust Emission

Thermal dust is dominated in foreground at higher frequencies $\geq 70\text{GHz}$. It is thermal emission from interstellar dust grains mostly made of graphite, silicates, and PAHs. Spectrum of thermal dust emission is defined by black-body of form $I_\nu = \nu^{\beta_d} B_\nu$ where B_ν is Planck spectrum. The temperature T is determined by the interstellar radiation field (heating) and efficiency of emitting far-infrared light (cooling) of the dust grains.

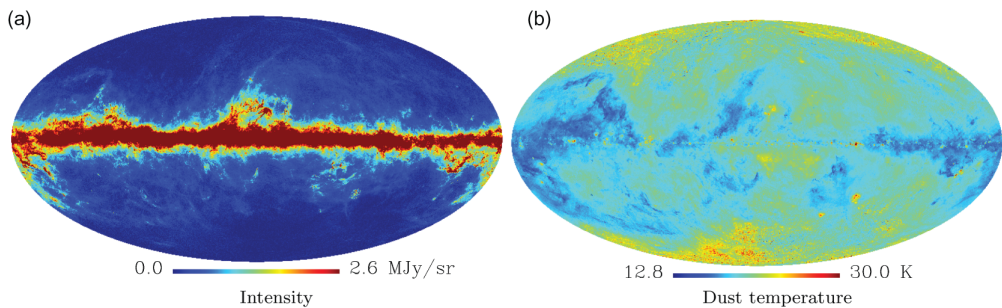


Fig. 2.4: (left) Thermal dust emission map at 353 GHz estimated by the Planck experiment using the Commander. (Right) Dust Temperature map estimated from modeling the IRIS 100 μm and the Planck HFI emission at 857 and 545GHz[22]

Detailed all sky maps of dust intensity and temperature have been released by the Planck (Fig.3). Along the galactic plane, a temperature gradient can

be seen from the outer galactic center from $T \approx 14 - 15k$ to $T \approx 19k$.

Photons emitted from thermal dust with a spherical shape can be polarized, with spin-axes aligned with interstellar magnetic field. WMAP satellite has observed the polarization fraction of dust emission is about 1% towards the galactic center and can be large as 6% away from center.

2.2.4 Spinning Dust Emission

Spinning dust emission is coming from tiny PHA particles spinning with dipole moment. This is anomalous emission at 20-60GHz. It is also nicknamed as "Foreground-X"[23]. The anomalous emission can be estimated by subtracting contribution of synchrotron, free-free, and thermal dust emissions from the WMAP frequency maps. It was found that in the WMAP K and Ka bands the spectral index of anomalous emission is $\beta_d \approx -2.5$.

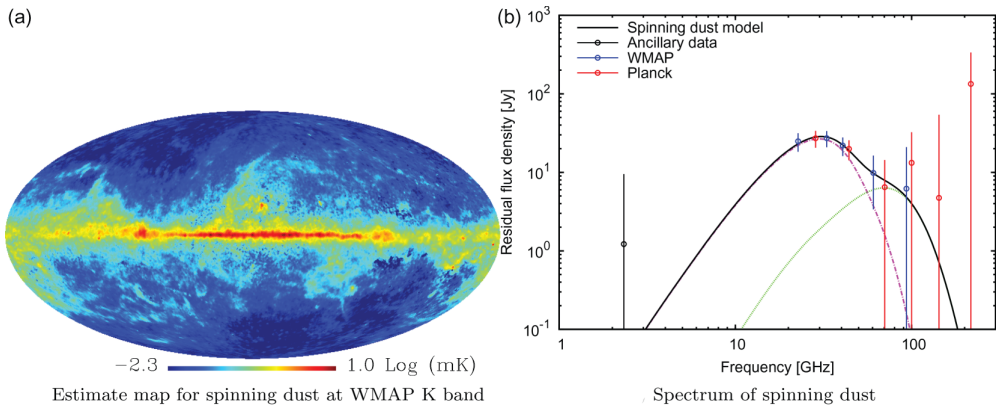


Fig. 2.5: (Left) Estimate of the anomalous emission at WMAP K-band[20]. (Right) Spectrum of anomalous emission in the ρ Ophiuchi molecular cloud after subtracting the best-fitting free-free, CMB and thermal dust components. The curves are the spinning dust model calculated using SPDUST for dense molecular gas and low-density atomic gas. Source: Plank Collaboration et al., A&A, 536, A6 2011 and DOI:10.1093/ptep/ptu065[24]

Polarization amplitude of spinning dust emission is small. There is another possible candidate for this anomalous emission is magneto-dipole emission from strongly magnetized grains.

2.2.5 CO Molecular Cloud Emission

Co molecular cloud emission is coming from rotational transition of carbon monoxide(CO). The frequencies of three rotational transitions of CO are $j=(1-0)$ at 115 GHz, $j=(2-1)$ at 230GHz and $j=(3-2)$ at 345 GHz are in the first, third and fourth transmission bands pf Planck's high frequency Instrument(HFI) which is 100, 217, 353 GHz. At high galactic latitude power spectrum of CO emission gives significant contribution.

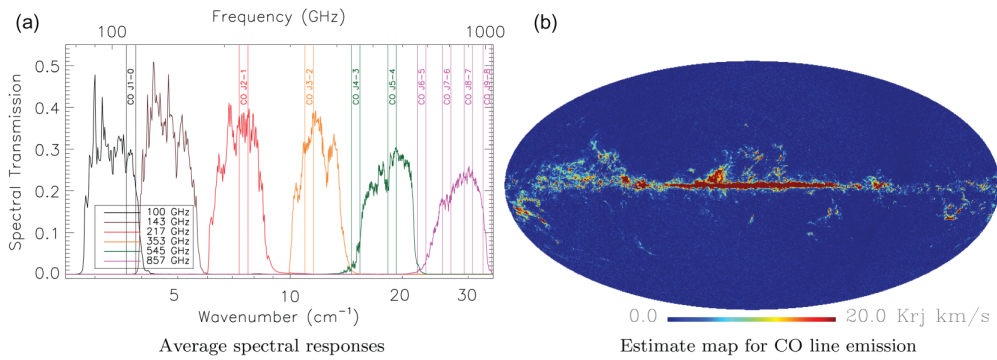


Fig. 2.6: (Left) The average spectral responses for the HFI bands. Vertical lines indicate the position of CO line emission. Source: Plank Collaboration et al., A&A, 536, A6 2011. (Right) The full sky view of CO line emission ($j = (1-0)$) obtained by planck. Source: DOI:10.1093/ptep/ptu065[24]

2.3 Cosmic Microwave Background(CMB)

cosmic microwave background (CMB) radiation is most important probe to study early universe and cosmology. In current cosmology CMB is most influential cosmological observation, and well recognized prime areal in astronomy and astrophysics in science community.

The cosmic microwave background (CMB) radiation was discovered in 1965 by the American physicist Arno Allan Penzias (1933) and the American astronomer Robert Woodrow Wilson (1936). CMB is coming from all directions of sky and considered as Raleigh radiation left after big bang and formation of our universe. Today the temperature of CMB is 2.7 degree above absolute zero. Now a days CMB radiation is considered as a best evidence of big bang model of cosmology.

According to theory, early universe was made up of plasma of proton, electron and baryons. Through Thomson scattering protons were continuously interacting with plasma. latter universe expanded and cooled adiabatically which cause to cool plasma and combine the electron and proton to form hydrogen atom. All this happened when universe was approximately 380000 years old and the temperature was approximately $3000K$. At this time universe become opac and photons starts traveling freely through the space. This entire process is called recombination or decoupling.

3. DESCRIPTION OF DATA

In this chapter in section 3.1 we will discuss about the data that we have used for our project, in section 3.2 we will discuss about smoothing of maps and in section 3.3 we will discuss about mask map that we have used for masking input maps.

3.1 WMAP Data And Templates

The Wilkinson Microwave Anisotropy Probe (WMAP) is a NASA Explorer mission which was launched on June 2001 to make fundamental measurements of cosmology that is to study the properties of our universe as whole. WMAP has been successful in producing our new standard model of cosmology. The WMAP determined the geometry, content, and evolution of the universe via a 13 arc-minute FWHM resolution full sky map of the temperature anisotropy of cosmic microwave background radiation.

Tab. 3.1: Table for wavelength, frequency, beam size etc. of different band.
Source: DOI:10.1088/0004-637X/717/2/825

	K-Band	Ka-Band	Q-Band	V-Band	W-Band
Wavelength(mm)	13	9.1	7.3	4.9	3.2
Frequency(GHz)	23	33	41	61	94
Bandwidth(GHz)	5.5	7.0	8.3	14.0	20.5
Number of Channels	4	4	8	8	16
Beam Size(deg)	0.88	0.66	0.51	0.35	0.22
System Temperature(K)	29	39	59	92	145
Sensitivity($mKsec^{\frac{1}{2}}$)	0.8	0.8	1.0	1.2	1.6

In this project we are using WMAP 9 year data which is six maps on five frequencies (23 GHz, 33 GHz, 41 GHz, 61 GHz, 94 GHz).

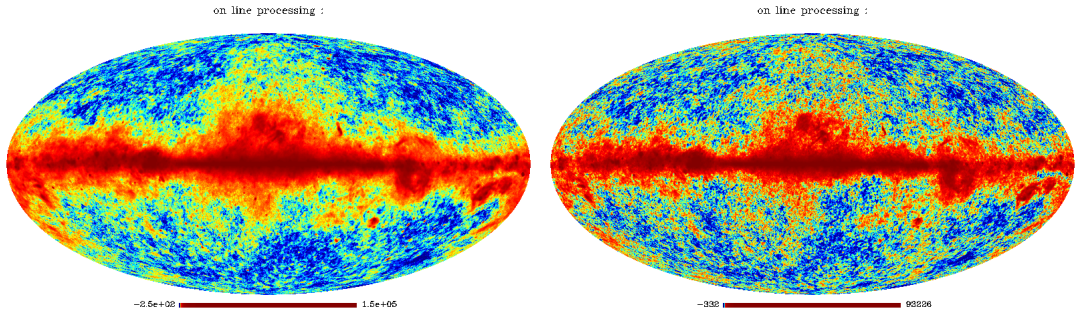


Fig. 3.1: (Left) WMAP K1-band map at 23GHz frequency. (Right) WMAP Ka1-band map at 33GHz frequency

In above figure 3.1, left image is WMAP's K-Band map at frequency 23 GHz and right image is WMAP's Ka1-Band map at frequency at 33 GHz as mentioned in the table 3.1. Above maps are in mole-wide projection. In maps the temperature is plotted with θ and ϕ which represent galactic latitude and longitude. In center line that is called galactic plane, the dark red region the temperature while the blue region refers the lower temperature. In galactic plane the free-free and thermal dust contamination is more which is clearly indicated by dark red region. The bar bellow the map is indication of the change in temperature with respect to average value of the temperature.

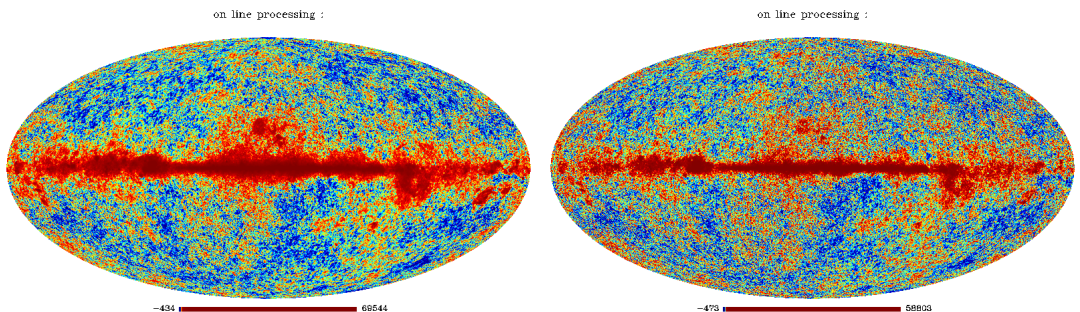


Fig. 3.2: (Left) WMAP Q1-band map at 41GHz frequency. (Right) WMAP V1-band map at 61GHz frequency

In above figure 3.2, left image is WMAP's Q1-Band map at frequency 41 GHz and right image is WMAP's V1-Band map at frequency at 61 GHz

as mentioned in the table 3.1.

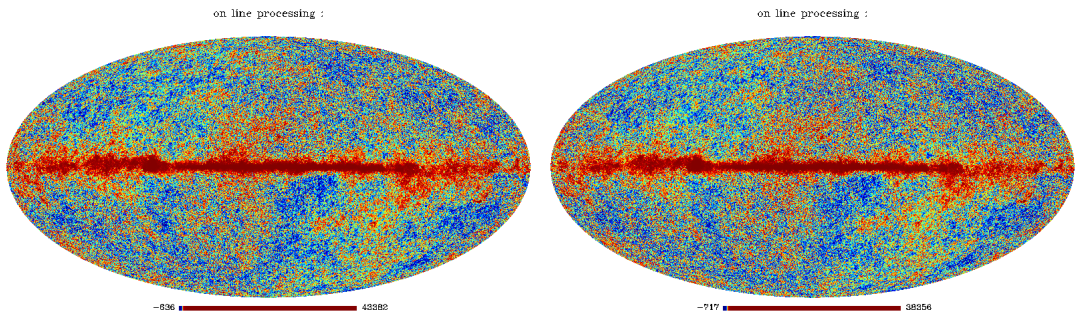


Fig. 3.3: (Left) WMAP W1-band map at 94GHz frequency. (Right) WMAP W2-band map at 94GHz frequency

In above figure 3.2, left image is WMAP's W1-Band map at frequency 94 GHz and right image is WMAP's W2-Band map at frequency at 94 GHz as mentioned in the table 3.1.

3.2 Smoothing of maps

Initially the WMAP data is provided in smoothed by some default beam value which varies over frequency and these maps have some initial nside value which is 512 for WMAP 9 year data. To increase computation time we need to downgrade the nside value as we downgraded all the maps to nside 64. After downgrading these maps get some noise. to remove this noise we need to smooth these maps by a same beam value for all maps. For my analysis we smoothed all maps by 3 deg.

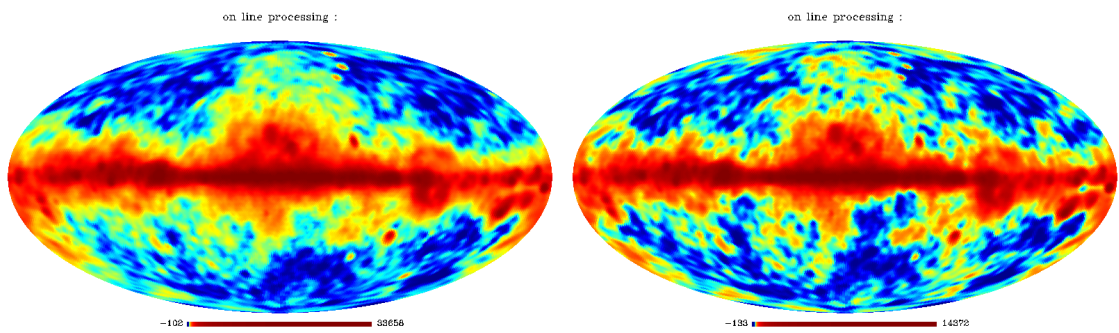


Fig. 3.4: (Left) WMAP K1-band map at 23GHz frequency, smoothed by 3^0 at $nside = 64$. (Right) WMAP Ka1-band map at 33GHz frequency, smoothed by 3^0 at $nside = 64$

In above figure 3.4, left image is WMAP's K-Band map at frequency 23 GHz, smoothed by 3^0 at $nside = 64$ and right image is WMAP's Ka1-Band map at frequency at 33 GHz, smoothed by 3^0 at $nside = 64$ as mentioned in the table 3.1.

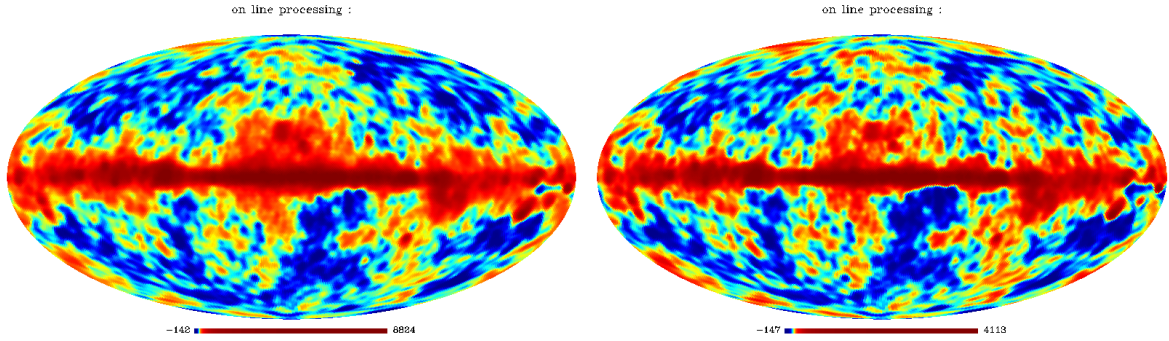


Fig. 3.5: (Left) WMAP Q1-band map at 41GHz frequency, smoothed by 3^0 at $nside = 64$. (Right) WMAP V1-band map at 64GHz frequency, smoothed by 3^0 at $nside = 64$

In above figure 3.5, left image is WMAP's V1-Band map at frequency 41 GHz, smoothed by 3^0 at $nside = 64$ and right image is WMAP's Q1-Band map at frequency at 61 GHz, smoothed by 3^0 at $nside = 64$ as mentioned in the table 3.1.

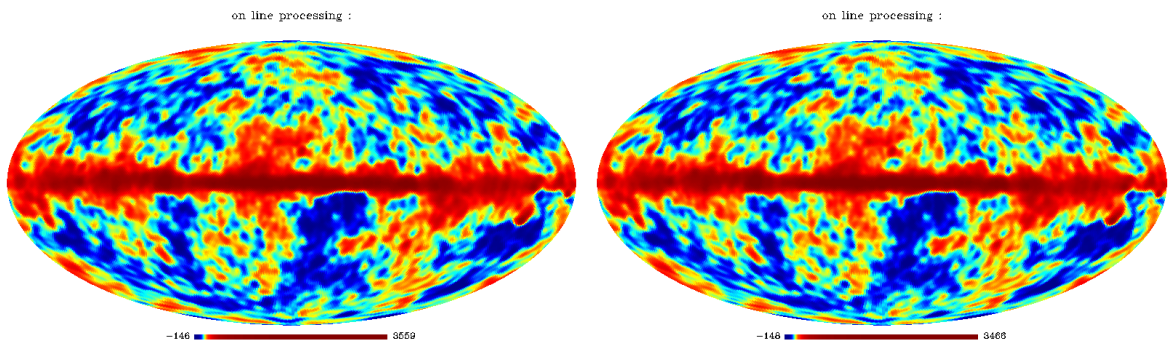


Fig. 3.6: (Left) WMAP W1-band map at 94GHz frequency, smoothed by 3^0 at $nside = 64$. (Right) WMAP W2-band map at 94GHz frequency, smoothed by 3^0 at $nside = 64$

In above figure 3.6, left image is WMAP's W1-Band map at frequency 94

GHz, smoothed by 3^0 at $nside = 64$ and right image is WMAP's W2-Band map at frequency at 94 GHz, smoothed by 3^0 at $nside = 64$ as mentioned in the table 3.1.

3.3 Mask

When we look in the central region of the maps, called as galactic plane, provided in Data section 3.1, is too much contaminated by foreground component, thermal dust. Apart from this central region there are lot of strong point sources are present in these maps. All these point sources can fade out haze signals as these point sources are much much stronger than haze signals.

To remove all these strong point sources and the strong signals present in galactic plane region we mask our input maps with kq85 mask provided by NASA's lambda website. The mask map is as follows

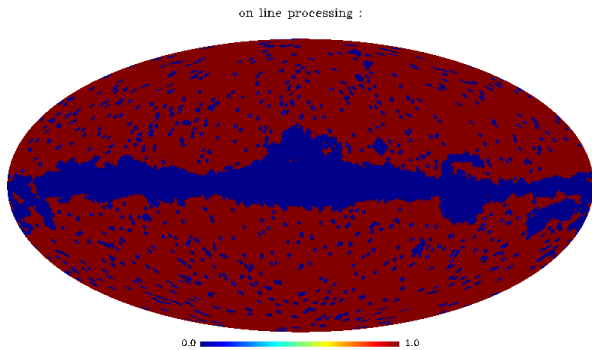


Fig. 3.7: KQ85 mask provided by WMAP smoothed by 3^0 at $nside = 64$

Mask values for each map pixel are provided in the N_{obs} field of the data file (the 'Temperature' field should be disregarded). A mask value of zero means the pixel is rejected; a value of one means the pixel is accepted. For temperature analysis, we have used the standard cut ("temperature_kq85") corresponds roughly to the "Kp2" cut in the 3-year data release.

4. ANALYSIS OF DATA

In this chapter in section 4.1 we will describe about power spectrum and weights calculation, in section 4.2 we will discuss about noise estimation and in section 4.3 we will discuss about χ^2 calculation.

4.1 Calculation of power spectrum and Weights

In this section we describe our procedure for estimating the power spectrum of the WMAP and weights for cleaned maps.

4.1.1 Cross-power spectrum estimation

We estimate the power spectrum by cross correlating pairs of foreground-cleaned maps. To remove detector noise bias we cross correlate two cleaned maps which do not have a common detector map. For example, cross correlating the two cleaned maps which are obtained from the individual maps (K, Q1, V1, W1, W2), respectively, yields a power spectrum with substantially reduced detector noise bias. A central mask is applied to each of the cleaned maps prior to cross correlation in order to remove residual contamination from the galactic region and resolved point sources. The alternative to cross correlation is to use auto-correlation and use a detector noise model to remove bias from the power spectrum. In the auto-correlation case the detector noise model uncertainty affects the mean of the cleaned power spectrum, whereas the cross-correlation method is advantageous since the power spectrum is not affected by the uncertainty in the noise model. The ba-

sic idea of the MASTER method is that removing a sky region effectively introduces uneven weighting of the pixels. Those removed have effectively zero weight and the rest have unit weight. Weighting a map in pixel space induces correlations between neighboring multipoles. The correlation of the multipoles is described by the coupling matrix which is determined by the geometry of the sky coverage. Moreover, the partial sky power spectrum of such a map has a lower bias because of the reduced coverage. The MASTER method removes bias from the partial sky power spectrum on the ensemble average by inverting the coupling matrix. We convert each of the 24 partial-sky cross-power spectra to full sky estimates using the coupling (bias) matrix corresponding to the central mask. The small scale systematic effects of beam and pixel smoothing are removed using appropriate circularized beam transform and pixel window functions. The resulting full sky cross-power spectra are then combined with equal weights into a single uniform average power spectrum. There exists some residual unresolved point source contamination in the uniform average power spectrum.

4.1.2 Estimation of weights for cleaned maps

To calculate weights we need shape-vectors. shape-vector calculation can be done by following formula.

$$sv(\nu) = g_\nu \left(\frac{\nu}{\nu_0} \right)^n \quad (4.1)$$

Where, $g_\nu = \frac{(e^x - 1)^2}{x^2 e^x}$ and $x = \frac{0.0662607004d \times \nu}{(1.38064852 \times 2.7255)}$, ν is frequency of the map. sv is shape-vector, which is further used to calculate weights.

Calculation of weights for any foreground component can be made by the making weights orthogonal of other foreground components.

$$WC_l W^T - \alpha WP^T - \beta WQ^T - \gamma WR^T = 0 \quad (4.2)$$

Where W is weights, $\{P, Q, R\}$ are shape-vectors, $\{\alpha, \beta, \gamma\}$ are constants, and C_l is power spectrum.

Taking differentiation with respect to W ,

$$2C_l W^T - \alpha P^T - \beta Q^T - \gamma R^T = 0$$

Further simplifying above equation by multiplying C_l^{-1} on both side, we get following equation.

$$2W^T = \alpha C_l^{-1} P^T + \beta C_l^{-1} Q^T + \gamma C_l^{-1} R^T$$

Further simplification by dividing by 2 on both side,

$$W^T = \frac{1}{2}[\alpha C_l^{-1} P^T + \beta C_l^{-1} Q^T + \gamma C_l^{-1} R^T] \quad (4.3)$$

Taking transpose of above equation,

$$(W^T)^T = \frac{1}{2}[\alpha C_l^{-1} P^T + \beta C_l^{-1} Q^T + \gamma C_l^{-1} R^T]^T$$

C_l^{-1} is a symmetric matrix. so $(C_l^{-1})^T = C_l^{-1}$

$$W = \frac{1}{2}[\alpha C_l^{-1} P + \beta C_l^{-1} Q + \gamma C_l^{-1} R] \quad (4.4)$$

To calculate weights for particular shape-vector, we will make other shape-vector orthogonal,

$$WP^T = \frac{1}{2}[\alpha C_l^{-1} PP^T + \beta C_l^{-1} QP^T + \gamma C_l^{-1} RP^T] = 1 \quad (4.5)$$

To remove Q component here we are making Q component orthogonal to weights by following equation,

$$WQ^T = \frac{1}{2}[\alpha C_l^{-1} PQ^T + \beta C_l^{-1} QQ^T + \gamma C_l^{-1} RQ^T] = 0 \quad (4.6)$$

To remove R component here we are making R component orthogonal to weights by following equation,

$$WR^T = \frac{1}{2}[\alpha C_l^{-1} PR^T + \beta C_l^{-1} QR^T + \gamma C_l^{-1} RR^T] = 0 \quad (4.7)$$

By solving above three equations 4.5, 4.6 and 4.7,

$$\begin{bmatrix} PC_l^{-1}P^T & QC_l^{-1}P^T & RC_l^{-1}P^T \\ PC_l^{-1}Q^T & QC_l^{-1}Q^T & RC_l^{-1}Q^T \\ PC_l^{-1}R^T & QC_l^{-1}R^T & RC_l^{-1}R^T \end{bmatrix} \begin{bmatrix} \alpha \\ \beta \\ \gamma \end{bmatrix} = \begin{bmatrix} 2 \\ 0 \\ 0 \end{bmatrix} \quad (4.8)$$

Now further simplifying equation 4.8,

$$\begin{bmatrix} \alpha \\ \beta \\ \gamma \end{bmatrix} = \begin{bmatrix} PC_l^{-1}P^T & QC_l^{-1}P^T & RC_l^{-1}P^T \\ PC_l^{-1}Q^T & QC_l^{-1}Q^T & RC_l^{-1}Q^T \\ PC_l^{-1}R^T & QC_l^{-1}R^T & RC_l^{-1}R^T \end{bmatrix}^{-1} \begin{bmatrix} 2 \\ 0 \\ 0 \end{bmatrix} \quad (4.9)$$

Now by solving matrix 4.9 we will get all constants α, β, γ . and using these constants in equation 4.4 we will get weights for map.

4.2 Noise Estimation

When data is recorded by WMAP satellite, it includes some instrumental noise in maps. During the analysis, removal of this instrumental noise is necessary.

Noise reduction can be done using standard deviation of the data. WMAP satellite make many observations for single co-ordinate value and also record this no of observations with respect to l . In WMAP 9 year data, the second column gives these number of observations.

standard deviation of maps,

$$\Delta_j^i = \sqrt{\sum_{i=1}^n \frac{\sigma_0^{i^2}}{nob_j^i}} \quad (4.10)$$

Where Δ is standard deviation, n is number of maps, σ_0 is FWHM, values $\sigma_0 = [1.429d, 1.466d, 2.245d, 3.314d, 5.899d, 6.562d]$ for (K1, Ka1, Q1, V1, W1, W2)respectively, nob is number of observations, and i is index over maps and j is index over l values.

Downgrade standard deviation maps to the same nside value as the

input maps have,

$$\Delta_j^i = \sqrt{\frac{\Delta_j^{i2}}{ratio}} \quad (4.11)$$

where $ratio = \frac{npix}{npix_{low}}$, $npix$ is number of pixels corresponding to nside of maps and $npix_{low}$ is number of pixels corresponding to downgraded nside value and $npix = 12 \times nside^2$.

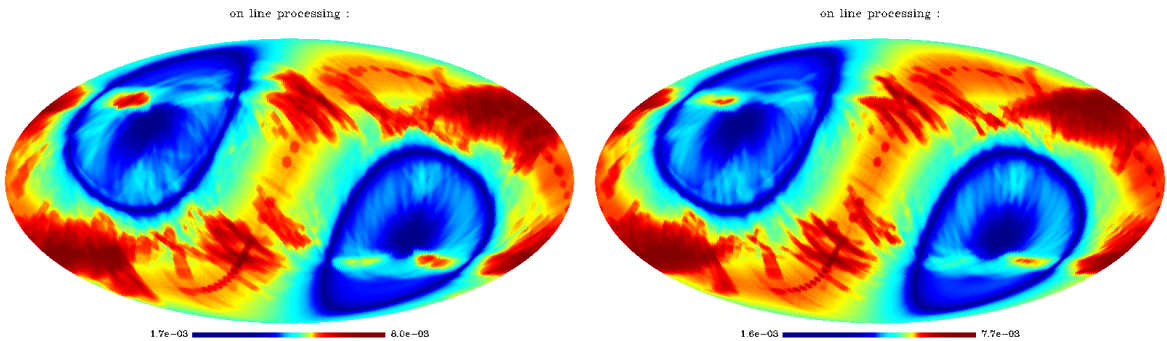


Fig. 4.1: All above maps are standard deviation maps for K1, Ka1, Q1, V1, W1 and W2 respectively

Further this standard deviation matrix is used to calculate simulated noise matrix. we calculated 10,000 simulated noise matrix for each frequency map.

$$\Delta N_i^j = N^j \times \Delta_i^j \quad (4.12)$$

Where ΔN is simulated noise maps, j is index over number of simulations and i is index over number of maps.

Now again we need to smooth these simulated noise maps by the same value that we used to smooth input maps. After smoothing we again recombine all simulated maps of same frequency band to single noise map for each frequency band.

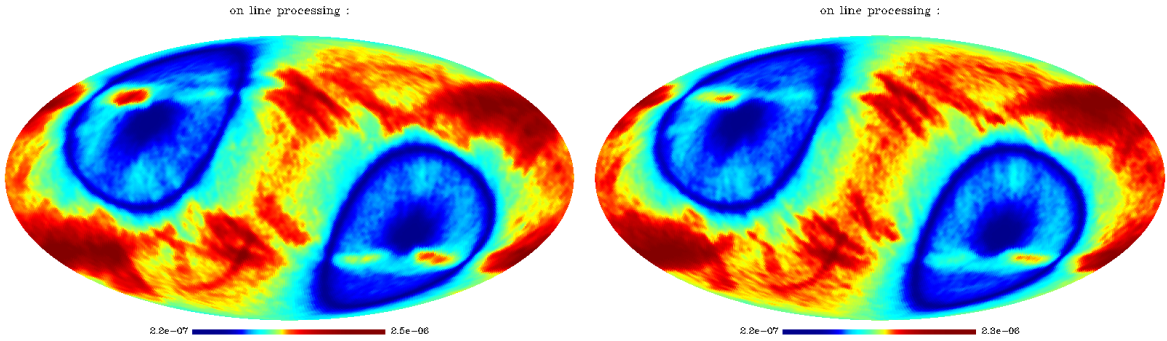


Fig. 4.2: All above maps are co-variance maps for K1, Ka1, Q1, V1, W1 and W2 respectively

Now using these noise maps we will calculate noise co-variance matrices.

Templates of components in pixel space,

$$\begin{aligned} \hat{D}\hat{M}(p) &= \sum_i W_{DM}^i T^i(p) & D\hat{M}_\nu(p) &= a_\nu^i \left(\frac{\nu^i}{\nu_0}\right)^{\beta_{DM}} \hat{D}\hat{M}(p) \\ \hat{D}(p) &= \sum_i W_D^i T^i(p) & \hat{D}_\nu(p) &= a_\nu^i \left(\frac{\nu^i}{\nu_0}\right)^{\beta_D} \hat{D}(p) \\ \hat{S}(p) &= \sum_i W_S^i T^i(p) & \hat{S}_\nu(p) &= a_\nu^i \left(\frac{\nu^i}{\nu_0}\right)^{\beta_S} \hat{S}(p) \end{aligned}$$

Where $\hat{D}\hat{M}(p)$ is dark matter template, $\hat{D}(p)$ is thermal dust template and $\hat{S}_\nu(p)$ is synchrotron template at pixel value p , ν is frequency, β_{DM} is dark matter spectral index, β_D is thermal dust spectral index, β_S is synchrotron spectral index and a_ν^i is shape vector at frequency ν for map i , W_{DM}^i , W_D^i & W_S^i are weights for dark matter, thermal dust and synchrotron respectively for map i .

Now from above equations we can convert templates in following equations,

$$D\hat{M}_\nu(p) = a_\nu^i \left(\frac{\nu^i}{\nu_0}\right)^{\beta_{DM}} \sum_i W_{DM}^i T^i(p) \quad (4.13)$$

$$\hat{D}_\nu(p) = a_\nu^i \left(\frac{\nu^i}{\nu_0}\right)^{\beta_D} \sum_i W_D^i T^i(p) \quad (4.14)$$

$$\hat{S}_\nu(p) = a_\nu^i \left(\frac{\nu^i}{\nu_0}\right)^{\beta_S} \sum_i W_S^i T^i(p) \quad (4.15)$$

Noise in pixel space can be calculated by using following equation,

$$N^i(p) = T^i(p) - [D\hat{M}_\nu^i(p) + D_\nu^i(p) + S_\nu^i(p)] \quad (4.16)$$

Now using $D\hat{M}(p)$ template, $\hat{D}(p)$ template and $\hat{S}_\nu(p)$ template from equation 4.13, 4.14 and 4.15 in equation 4.16 we get following equation.

$$\begin{aligned} N^i(p) &= T^i(p) - [a_\nu^i \left(\frac{\nu^i}{\nu_0}\right)^{\beta_{DM}} \sum_j W_{DM}^j T^j(p) + a_\nu^i \left(\frac{\nu^i}{\nu_0}\right)^{\beta_D} \sum_j W_D^j T^j(p) + \\ &\quad a_\nu^i \left(\frac{\nu^i}{\nu_0}\right)^{\beta_S} \sum_j W_S^j T^j(p)] \\ N^i(p) &= \underbrace{[1 - a_\nu^i \left\{ \left(\frac{\nu^i}{\nu_0}\right)^{\beta_{DM}} W_{DM}^i + \left(\frac{\nu^i}{\nu_0}\right)^{\beta_D} W_D^i + \left(\frac{\nu^i}{\nu_0}\right)^{\beta_S} W_S^i \right\}] T^i(p)}_{for i=j} \\ &- a_\nu^i \underbrace{\sum_{i \neq j} \left\{ \left(\frac{\nu^i}{\nu_0}\right)^{\beta_{DM}} W_{DM}^j + \left(\frac{\nu^i}{\nu_0}\right)^{\beta_D} W_D^j + \left(\frac{\nu^i}{\nu_0}\right)^{\beta_S} W_S^j \right\} T^j(p)}_{for i \neq j} \end{aligned}$$

Above equation explains the noise variance of the map.

Noise co-variance can be calculated by squaring above equation,

$$\begin{aligned} N_{pp'}^{i,D} &= [1 - a_\nu^i \left\{ \left(\frac{\nu^i}{\nu_0}\right)^{\beta_{DM}} W_{DM}^i + \left(\frac{\nu^i}{\nu_0}\right)^{\beta_D} W_D^i + \left(\frac{\nu^i}{\nu_0}\right)^{\beta_S} W_S^i \right\}]^2 \langle T^i(p) | T^i(p) \rangle \\ &- (a_\nu^i)^2 \sum_{i \neq j} \left\{ \left(\frac{\nu^i}{\nu_0}\right)^{\beta_{DM}} W_{DM}^j + \left(\frac{\nu^i}{\nu_0}\right)^{\beta_D} W_D^j + \left(\frac{\nu^i}{\nu_0}\right)^{\beta_S} W_S^j \right\}^2 \langle T^i(p) | T^j(p) \rangle \end{aligned}$$

Further simplifying above equation leads to following equation.

$$N_{pp'}^{i,D} = [1 - \tilde{W}_i^i]^2 N_{pp'}^i + \sum_{i \neq j} \tilde{W}_i^i \tilde{W}_j^j N_{pp'}^j \quad (4.17)$$

Where, $\tilde{W}_i^i = a_\nu^i \left\{ \left(\frac{\nu^i}{\nu_0}\right)^{\beta_{DM}} W_{DM}^i + \left(\frac{\nu^i}{\nu_0}\right)^{\beta_D} W_D^i + \left(\frac{\nu^i}{\nu_0}\right)^{\beta_S} W_S^i \right\}$
and $\tilde{W}_i^j = (a_\nu^i) \left\{ \left(\frac{\nu^i}{\nu_0}\right)^{\beta_{DM}} W_{DM}^j + \left(\frac{\nu^i}{\nu_0}\right)^{\beta_D} W_D^j + \left(\frac{\nu^i}{\nu_0}\right)^{\beta_S} W_S^j \right\}$

$N_{pp'}^{i,D}$ is the noise co-variance matrix of i^{th} (j^{th}) input frequency maps.
This noise co-variance matrix will be further used in χ^2 calculation.

4.3 χ^2 Calculation

In this process we were sampling spectral index of components (Dark Matter, Synchrotron, free-free), monopole and dipoles simultaneously. Out of these samples the best sample, to generate best dark matter map, can be estimated by the χ^2 calculation.

χ^2 can be calculated by using noise co-variance matrix in equation (4.17) by following formula,

$$\chi^2 = \frac{1}{N} \sum_{i,p,p'} (Q_i(p) - \tilde{Q}_i(p)) (N^{i,D})_{pp'}^+ (Q_i(p') - \tilde{Q}_i(p')) \quad [25] \quad (4.18)$$

Where $(N^{i,D})_{pp'}^+$ is Moore-penrose generalized inverse of $N_{pp'}^{i,D}$ and $N = n_b \times N_{pix}$ denotes total number of surviving pixels counting for all frequency bands.

In our analysis we are only weighting spectral indices of two components. So the equation (4.18) transforms in following equation.

$$\chi^2 = \frac{1}{N} (T^i(p) - DM^i(p) - S^i(p)) (N^{i,D})_{pp'}^+ (T^i(p) - DM^i(p) - S^i(p)) \quad (4.19)$$

Where $T^i(p)$ is input map template, $DM^i(p)$ is constructed dark matter map, $S^i(p)$ is constructed synchrotron map and $(N^{i,D})_{pp'}^+$ is Moore-penrose generalized inverse of $N_{pp'}^{i,D}$.

χ^2 depends on dark matter spectral index β_{DM} , synchrotron spectral index β_S , monopole value and spherical Harmonics (To generate dipole maps) a_{10} & a_{11} . The best fit values for all parameters are which together minimizes χ^2 given by equation (4.19).

5. METHODOLOGY

In this section we will describe the step-wise methodology of construction of dark matter and synchrotron maps. we first used simple subtraction technique and then to enhance result we used Marcov Chain Monte Carlo approach.

5.1 Simple Subtraction Technique

In this technique first we constructed foreground templets and then subtracted from input maps to get haze signals.

5.1.1 Only CMB is removed

In this process we used WMAP data (K1, Ka1, Q1, V1, W1, W2 band maps) described in section 3.1. These maps have some initial nside value (for WMAP it is 512 by default), to increase computation time we need to downgrade these maps. Downgrading can be done by Healpix [66] package command *UD_GRADE, map_in, map_out,[bad_data=, help=, nside_out=, order_in=, order_out=, pessimistic=]* . As we know these maps are already smoothed by some initial beam value which is by default provided by NASA's website [23], so we need to smooth them by some beam value which will be decided by the noise of the map because smoothing is done to reduce noise after downgrading maps. Smoothing is can be done as described in section 3.2. After smoothing we subtracted Cosmic Microwave Background (CMB) Map from these smoothed input maps. CMB map are generated by commander[56] program of plank mission and maps is given bellow.

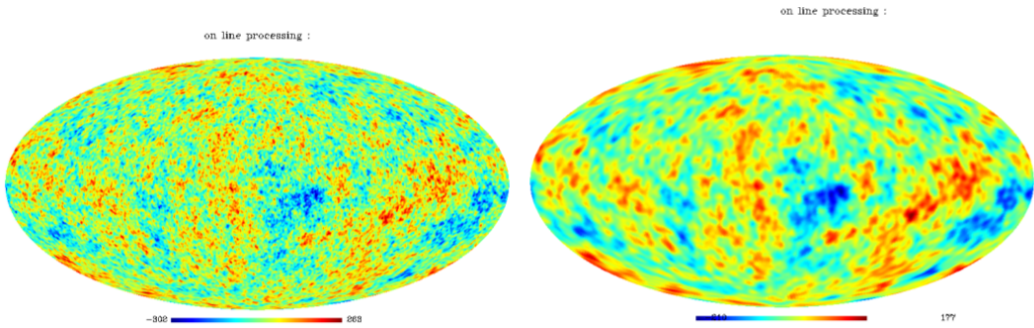


Fig. 5.1: CMB maps reproduced from commander program of planck collaboration. (Left) CMB map smoothed by 1° at $nside = 256$, (Right) CMB map smoothed by 3° at $nside = 64$

In above cmb maps left one is generated from commander program of plank mission and smoothed by 1° at $nside = 256$. and the right one is downgraded map at $nside = 64$ of left map by using `ud_grade` syntax 5.1.1 smoothed by 3° .

After subtracting these cmb maps 5.1.1 from downgraded input maps, we applied KQ_85 3.3 mask provided in WMAP data by NASA described in section 3.3. Now the input maps are ready to calculate weights and construct maps. Weights are constructed by process explained in subsection 4.1.2. These weights are used in `clean.pro` code to construct dark matter maps. Further χ^2 calculation is made by the process described in section 4.3 and the final result is published in section 6.1.

5.1.2 CMB and monopoles are removed

All the process is same as described in above section 5.1.1. Here we removed one extra contaminating component of monopole. Monopole values are taken from paper are 2.4, 5.6, 3.5, 2.7 and 3.9 for K, Ka, Q, V and W respectively. These monopole values are directly subtracted from the input maps and then again dark matter maps are constructed and χ^2 calculation is made. Results for this process is published in section 6.2.

5.1.3 CMB, monopoles and free-free are removed

In this section again all the process is same as described in above sub-sub-section 5.1.2. Here we remove one foreground component free-free emission by making weights orthogonal to free-free emission. The free-free map that we used is generated by commander program of plank collaboration. Free-free map used in this process is given bellow.

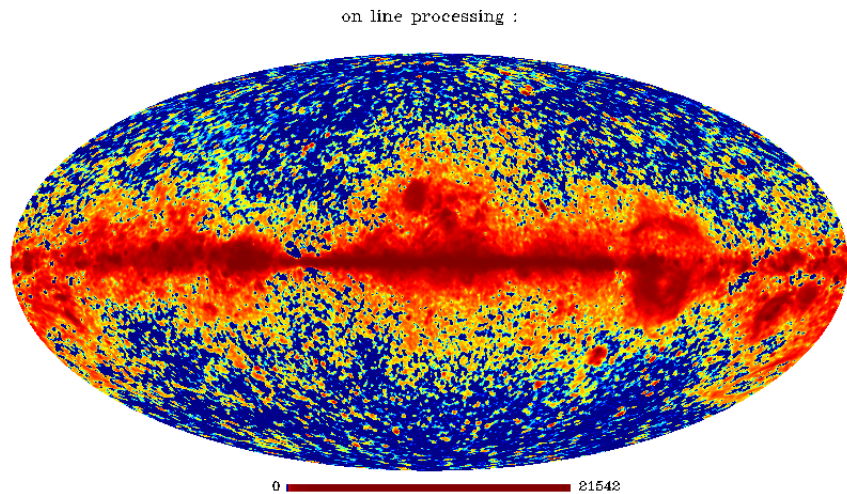


Fig. 5.2: Free-Free maps reproduced from commander program of Planck collaboration.

Above free-free map is smoothed by 1° at $nside = 256$. In the program **clean_v1.pro**, which is used to construct dark matter maps in this process, this free-free map is downgraded to $nside = 64$ and smoothed at 3° . The results for this process is described in section 6.3.

5.2 Use of Markov Chain Monte Carlo Approach to Enhance Results

Results achieved from simple subtraction technique, described in subsection 5.1, are not very good as lot of contamination is still present in the constructed dark matter/haze signal maps. The major drawback of previous technique is to not able to include more parameters simultaneously to

improve results and one more draw back was computation time, as we are sampling the spectral index in entire range, which is increasing computation time and that to includes computational error.

To tackle above problems we decided to use Markov Chain Monte Carlo Approach. In this approach instead of sampling on entire spectral index we picked spectral indexes randomly and sampled them. In this process the next sample is decided by the result of previous sampled value which increases efficiency and decreases computation time. The major advantage of this process is that we can sample all parameters (Spectral index of foreground components (dark matter, synchrotron, free-free), monopole values and Dipole values) at the same time.

5.2.1 Markov Chain Monte Carlo Approach

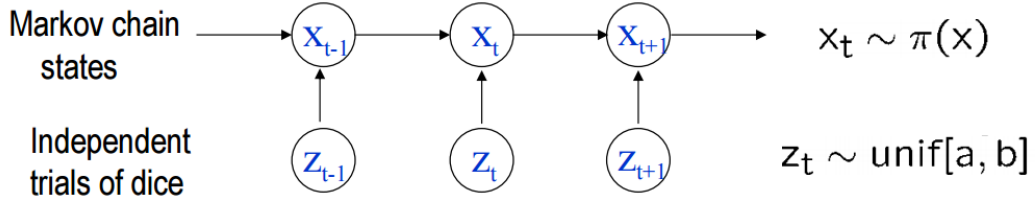
A Markov chain is a mathematical model for stochastic systems whose states, discrete or continuous, are governed by a transition probability. The current state in a Markov chain only depends on the most recent previous states, e.g for 1st order Markov chain.

$$X_t | X_{t-1}, \dots, X_0 \approx P(X_t | X_{t-1}, \dots, X_0) = P(X_t | X_{t-1}) \quad (5.1)$$

The Markovian property means locality in space or time, such as Markov random fields and Markov chain. Indeed, a discrete time Markov chain can be viewed as a special case of the Markov random fields (causal and 1-dimensional).

A Markov chain is often denoted by (Ω, ν, K) for state space, initial and transition prob.

Markov Chain Monte Carlo is a general purpose technique for generating fair samples from a probability in high-dimensional space, using random numbers (dice) drawn from uniform probability in certain range. A Markov chain is designed to have $\pi(x)$ being its stationary (or invariant) probability.



For our project we used Markov Chain Monte Carlo Metropolis-Hastings technique. The detailed algorithm is given below which is used in this project.

Lets take some function $f(x)$ and initial x value is x_0

- 1) now draw a uniform-deviate between -20 to 20 for x .
- 2) calculate $R = \frac{f(x)}{f(x_0)}$
- 3) if $R < 1$, then accept x and $x_0 = x$
- 4) if $R > 1$, then draw another uniform-deviate between 0 and 1 which is equal to r ,
- if $r < R$ accept x and go to (1)
- else go to (1)

5.2.2 Sampling of Dipoles

In this sub-section we will describe about the dipole parameter sampling by using Markov Chain Monte Carlo approach (discussed in sub-section 5.2.1).

To remove dipoles from the input maps (3.1) we have to generate dipole maps. Dipole maps can be generated by using spherical harmonics and Legendre polynomial function. Legendre function can be generated in IDL (Interactive Data Language) by using following command.

$$Y_{10} = \text{spher_harm}(\theta, \phi, l, m, /double)$$

And spherical harmonics values will be sampled by Markov Chain Monte Carlo method.

Dipole map can be generated by following formula,

$$f(\theta, \phi) = a_{1,0}Y_{1,0}(\theta, \phi) + a_{1,-1}Y_{1,-1}(\theta, \phi) + a_{1,1}Y_{1,1}(\theta, \phi)$$

we know,

$$a_{l,-m} = (-1)^m a_{lm}^*$$

$$Y_{l,-m} = (-1)^m Y_{lm}^*$$

So,

$$f(\theta, \phi) = a_{1,0}Y_{1,0}(\theta, \phi) + (-1)^1 a_{1,1}(-1)^1 Y_{1,1}(\theta, \phi) + a_{1,1}Y_{1,1}(\theta, \phi)$$

$$f(\theta, \phi) = a_{1,0}Y_{1,0}(\theta, \phi) + 2\text{Re}(a_{1,1}Y_{1,1}(\theta, \phi)) \quad (5.2)$$

Using above equations we can generate sampled dipole maps as given bellow figure.

on line processing :

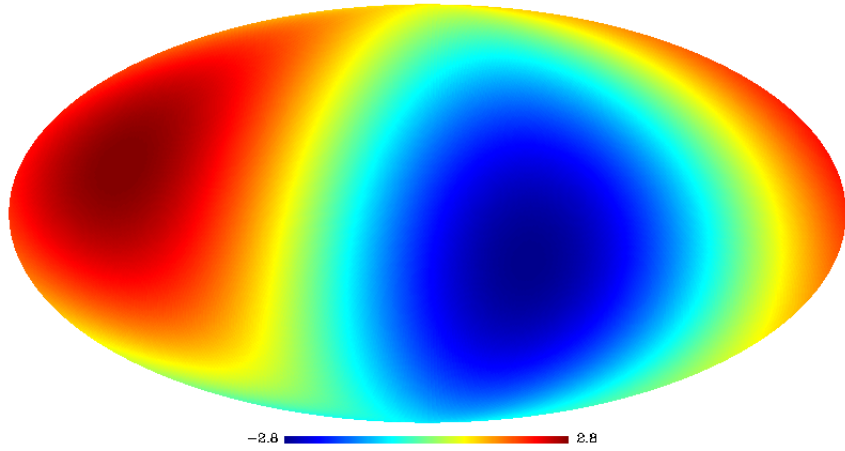


Fig. 5.3: Dipole map at $nside = 64$

5.2.3 Sampling of Spectral Indices and Monopoles

In this subsection we will describe the process of sampling of monopoles and Spectral indexes of foreground components.

The monopole values are sampled by generating uniform-deviate between -10 to 10 and we defined the upper and lower bound with this uniform-deviate. The initial values for monopole are mono 1.80, 6.30, 5.0, 1.50, and 4.10 for K1, Ka1, Q1, V1, and W bands respectively.

In foreground spectral index sampling, synchrotron emission is sampled with initial value of $\beta_S = -2.80$ and dark matter is sampled with initial value of $\beta_{DM} = -2.34$ by using Marcov chain Monte Carlo approach described in section 5.2.1.

6. RESULTS

In this chapter we will discuss the results, we generated after implementing the methodology described in chapter 5. Also we will discuss results step-wise and we will give proper explanation for those results.

6.1 Only CMB is subtracted

We first started with the subtraction of CMB from input maps smoothed by 3 degree. After re-moving CMB we and using liner combination of all maps and generated dark matter maps as shown bellow.

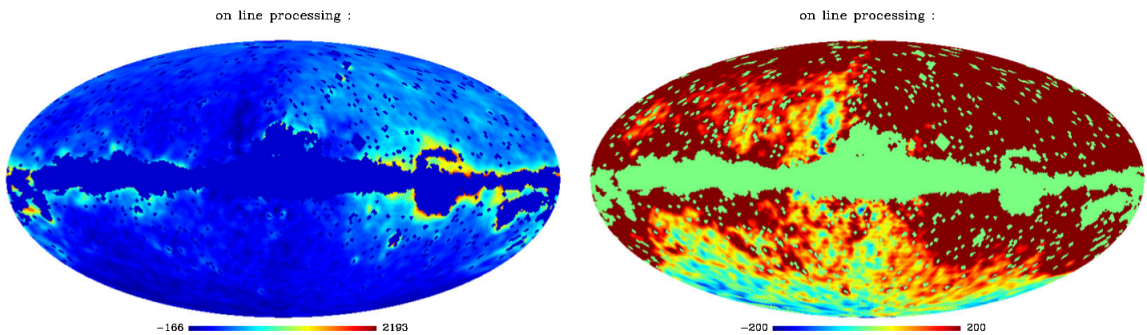


Fig. 6.1: Constructed dark matter maps at $\beta_{DM} = -2.56$ and $\beta_S = -2.80$

Left map in image is projection of dark matter without any limit of pixels at spectral index of dark matter -2.56 (which is reported in papers) and synchrotron 2.80. Right map in image is projection of dark matter with pixel range -200 to 200 at spectral index of dark matter -2.56 (which is reported in papers) and synchrotron -2.80. Central region of the maps is masked by a central mask provided by WMAP which is KQ85 mask. As we can see in above both maps lot of negative pixels and free free contamination

is present. The dark region in right map is contamination by some strong sources and dark blue region in the map is because of over-subtraction of signals. It is because we are not on the correct side of spectral index.

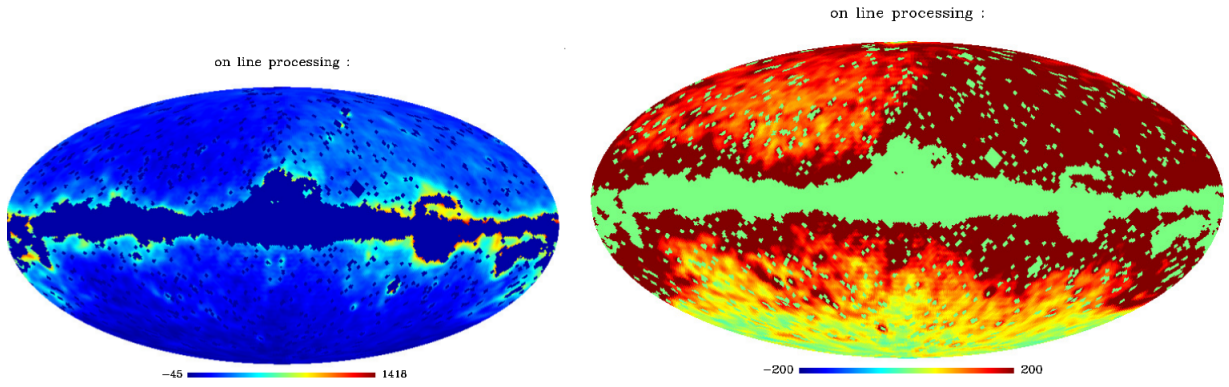


Fig. 6.2: Constructed dark matter maps at $\beta_{DM} = -2.56$ and $\beta_S = -3.10$

Left map in image is projection of dark matter without any limit of pixels at spectral index of dark matter -2.56 (which is reported in papers) and synchrotron -3.10. Right map in image is projection of dark matter with pixel range -200 to 200 at spectral index of dark matter -2.56 (which is reported in papers) and synchrotron -3.10. As we can see in above both maps thermal dust (dark region in galactic plane) and free-free contamination is present and it was expected as no free free, thermal dust emission is removed from input-maps. In this contamination Haze signal is hidden and not clearly visible. These maps are also contaminated with monopole and dipole. Our next step is to remove thermal dust. we also calculated χ^2 for each combination of spectral indexes and find the minima of this. this will give us the best fit map of dark mater corresponding to spectral index.

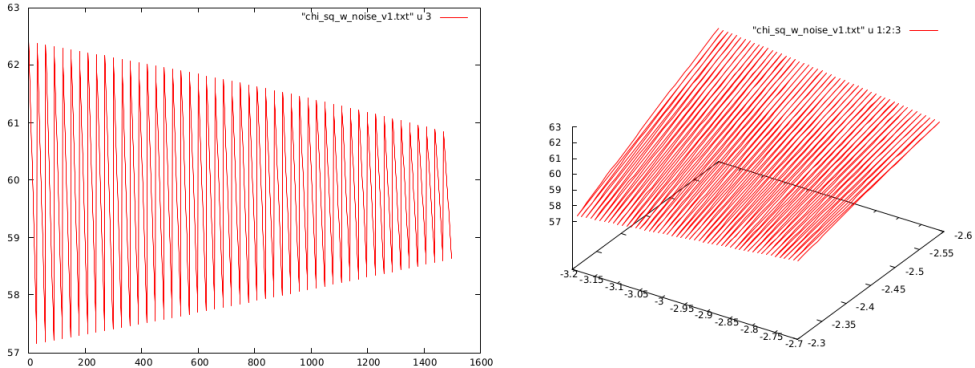


Fig. 6.3: Index vs χ^2 plot. (Left graph) on x-axis index values are plotted and on y-axis χ^2 values are plotted. (Right graph) on x-axis β_{DM} values are plotted, on y-axis β_S values are plotted and χ^2 values are plotted on z-axis.

In above χ^2 plots we can see there is no global minima in the 2-D plot of χ^2 . That means there no such spectral index value for which construction of best fit map is possible. That is because of presence of foreground emission, monopoles, dipole and detector noise present in maps.

6.2 CMB and Monopoles are subtracted

Now in this step we subtracted CMB and remove monopole from the input maps and then again generated the dark matter maps.

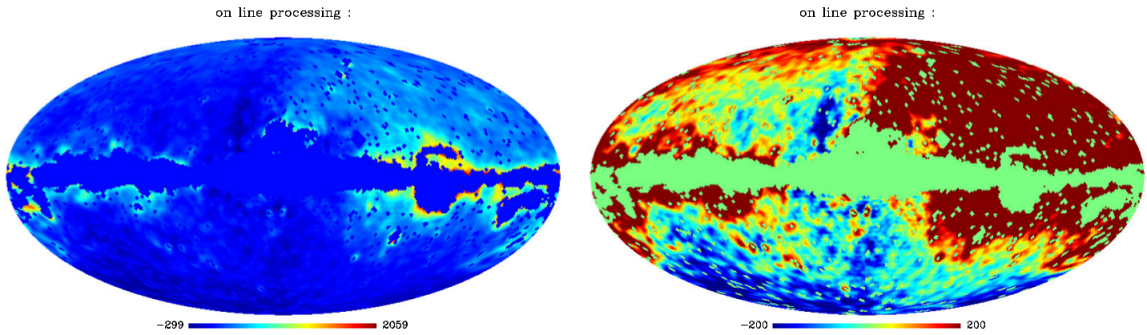


Fig. 6.4: Constructed dark matter maps at $\beta_{DM} = -2.56$ and $\beta_S = -2.80$

Again In above two maps it is clearly visible that it is still contaminated with free and thermal dust and also dark matter signals are not correctly visible because we are not on the correct side of spectral index. But this map is still on better side than last map as the monopole signals are removed from the map.

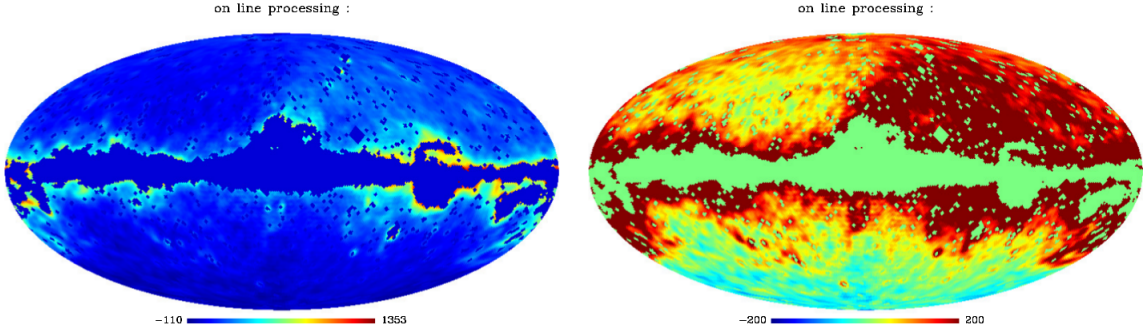


Fig. 6.5: Constructed dark matter maps at $\beta_{DM} = -2.56$ and $\beta_S = -3.10$.

In above two maps we can see some faint signals at the center of galactic plane but still it is contaminated with very strong thermal dust and free free emission. These maps are less contaminated as compare to last maps, that's why the faint signals are visible. as we will keep subtracting the contamination from the maps the visibility of the signals will increase.

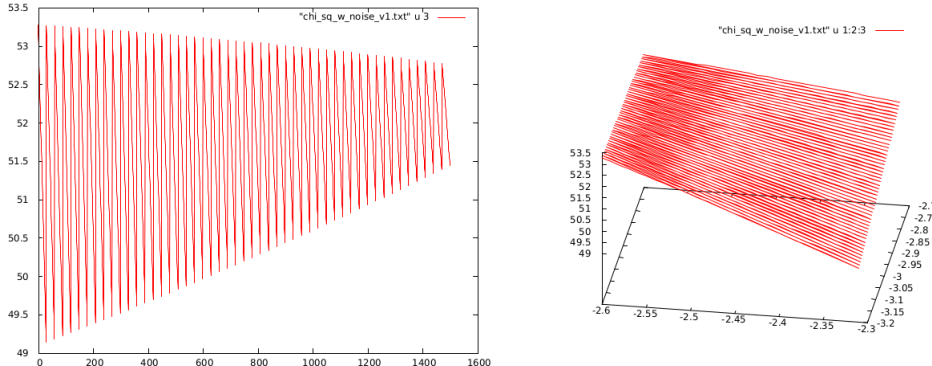


Fig. 6.6: Index vs χ^2 plot. (Left graph) on x-axis index values are plotted and on y-axis χ^2 values are plotted. (Right graph) on x-axis β_{DM} values are plotted, on y-axis β_S values are plotted and χ^2 values are plotted on z-axis.

In above χ^2 2-D plot again there is no global minima so there is no spectral for which we can construct a fit map. Still lot of fore ground contamination is present in these maps. Again these maps require more filtering.

6.3 CMB, Monopoles and Thermal Dust are subtracted

In this step we make weights orthogonal to thermal dust at spectral index 1.7 and then again reconstructed dark matter maps. By making weights orthogonal to thermal dust spectral index the thermal dust contamination will be subtracted from the maps.

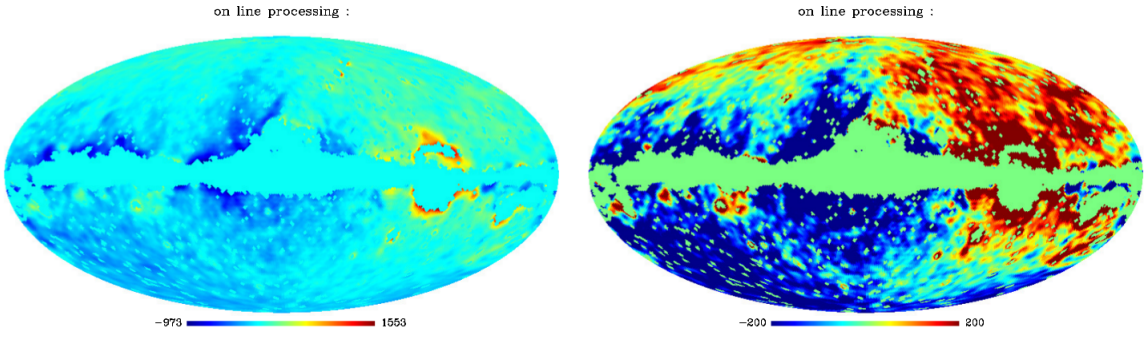


Fig. 6.7: Constructed dark matter maps at $\beta_{DM} = -2.56$ and $\beta_S = -2.80$

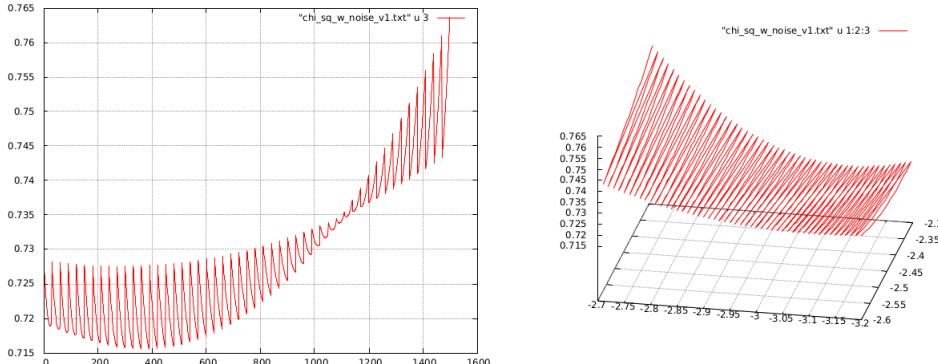


Fig. 6.8: Index vs χ^2 plot. (Left graph) on x-axis index values are plotted and on y-axis χ^2 values are plotted. (Right graph) on x-axis β_{DM} values are plotted, on y-axis β_S values are plotted and χ^2 values are plotted on z-axis.

In above two maps we can see that signals are not present because it is now contaminated with dipole moment. There are many possible cause behind this, of course dipole moment is one cause, but another cause that play major role is choice of correct spectral index value. To get correct spectral index value we need to look at χ^2 plot. The value which gives the global minima will give the correct choice of spectral index.

In above χ^2 plot a global minima is present at index value 400, which corresponds to spectral index values -2.56 and -3.10 for dark matter and synchrotron respectively. Now we will make dark matter maps for these spectral index value.

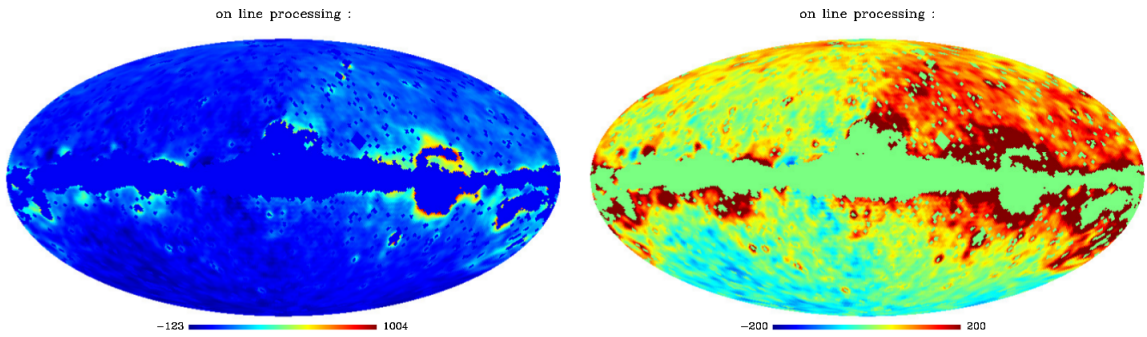


Fig. 6.9: Constructed dark matter maps at $\beta_{DM} = -2.56$ and $\beta_S = -3.10$.

In above two maps we can see some strong signals of dark matter haze at the center of galactic plane. But still lot of contamination of free-free, dipoles and other sources.

6.4 Results using Markov Chain Monte carlo Approach

Results provided in previous section was no that good because of lot of dipole and free-free contamination, though other contamination (emission due to other strong sources, spinning dust emission and CO molecular emission) were present in the maps but these two were the major contamination which were fading out the haze signals. After using Markov Chain Monte Carlo approach we tried to remove these signals and the resulting maps as follows.

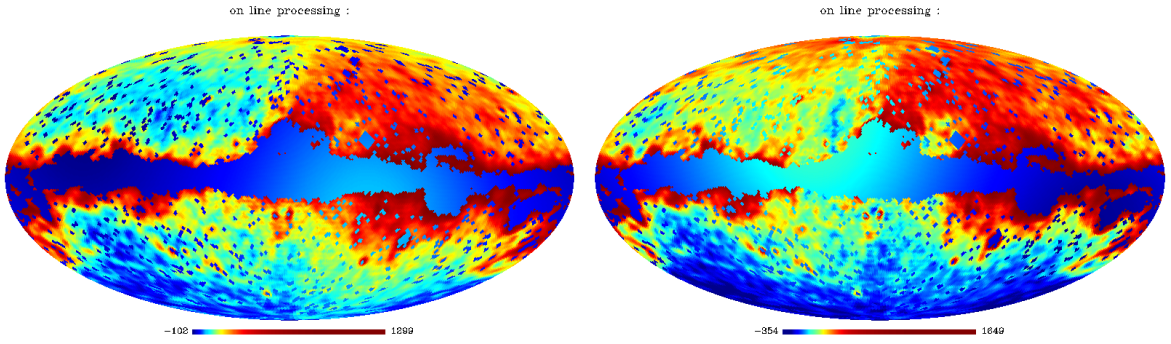


Fig. 6.10: Constructed dark matter maps at (left) $\beta_{DM} = -2.46$ and $\beta_S = -2.80$ and (Right) $\beta_{DM} = -2.34$ and $\beta_S = -2.70$ while using MCMC approach

In the above maps though free-free emission is removed but still dipole contamination is present and the possible cause behind this is not a proper choice of spectral index. Using Markov Chain Monte Carlo approach we sampled different spectral indexes and tried to calculate χ^2 , and the value at which χ^2 converges gives best map for haze signals. The χ^2 plot is as follows.

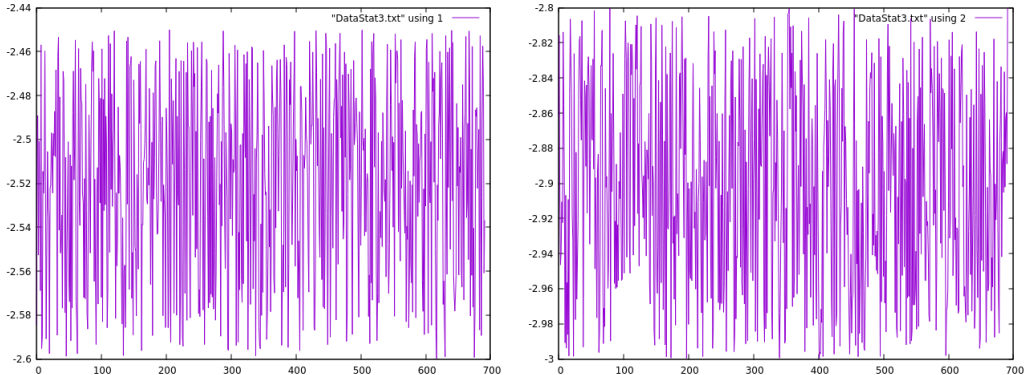


Fig. 6.11: Index vs Spectral index plot (left) for dark matter spectral index and (right) synchrotron spectral index plot. Index values are plotted on x-axis and spectral index values are plotted on y-axis

In above two plots the left (Dark Matter spectral Index) plot the values are varying from -2.46 to -2.58 and the average of number of values is about -2.52 & right plot (Synchrotron Spectral Index) plot the values are varying from -2.8 to -3.0 and the average of number of values is about -2.9. Hence at these spectral index values the dark matter map will have best fit map. before going to map we have to look at χ^2 values.

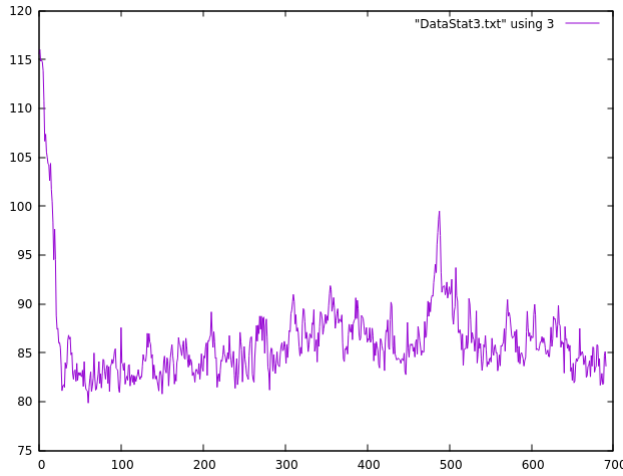


Fig. 6.12: χ^2 plot: index vs χ^2 . On x-axis index values are plotted and on y-axis χ^2 values are plotted.

In above χ^2 plot we can clearly see that χ^2 values started from 115 and very soon it converges in range of 80 and start fluctuating in between 80 to 85, mean value to these χ^2 is about 83 which again is in the spectral range of -2.52 and -2.9 for dark matter and synchrotron respectively. Now we will produce dark matter/ haze signal maps for these values and maps are as follows.

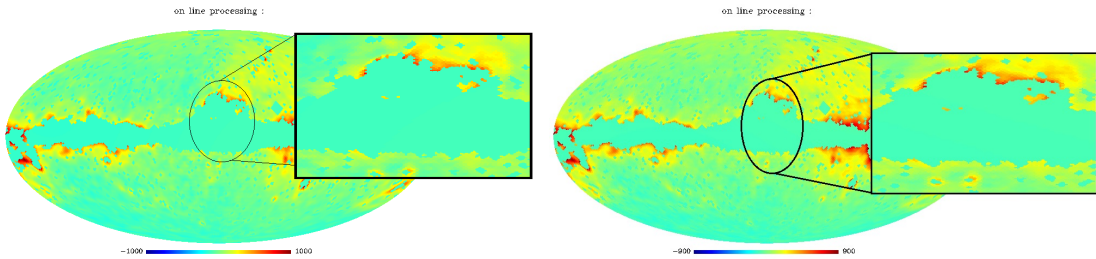


Fig. 6.13: Constructed dark matter maps at (left) $\beta_{DM} = -2.52$ and $\beta_S = -2.90$ and (right) $\beta_{DM} = -2.53$ and $\beta_S = -2.90$

In above dark matter maps we can see that contamination is almost removed and the signal visible at galactic center are likely to be a haze/bubble. Though a little contamination is present in these maps but that is fine because removal of contamination completely is not possible there is quite good possibility of residual contamination which may be because of computational errors.

7. SUMMARY

In this report, we have presented an evidence of WMAP Haze/Bubble from the WMAP nine-year data. The Haze morphology and spectrum are very similar to the reported morphological and spectrum in previous researches. Also with haze signals we have constructed synchrotron templates and estimated correct spectral index of synchrotron, $\beta_S = -2.90$. We have produced haze signals at spectral index, $\beta_{DM} = -2.52$.

We have used modified *Iterative Linear Combination (ILC)* of maps and produced Haze signals at spectral index, $\beta_{DM} = -2.56$ & synchrotron maps at spectral index, $\beta_S = -3.10$. We also illustrated that only using modified *ILC* of maps proper construction of map is very difficult as we in this process we can not add many parameters, it is limitation of my modified *ILC*. We have also shown that how we can use *Markov Chain Monte Carlo's Metropolis-Hasting technique* to enhance the results and construct better maps. We have constructed Haze/Bubble signal map by implementing *Markov Chain Monte Carlo's Metropolis-Hasting technique* and found dark matter spectral index $\beta_{DM} = -2.52$ and also constructed synchrotron map and estimated correct spectral index $\beta_S = -2.90$. We also illustrated that how we can add some more parameter to remove from input maps. We removed monopole, dipole contamination from map by sampling them using MCMC approach. We have calculated χ^2 calculation technique in this report to estimate best sample out of millions of samples generated. We have also illustrated how we can calculate noise for the input maps and remove them from the maps.

In this project we used only WMAP maps to construct dark matter maps. WMAP collected data on low frequency band and using WMAP data removal of all contamination completely is not possible. In future we

will use Plank HFI(High Frequency Instrument) maps to completely remove foreground contamination. In future we are planing to use WMAP maps and plank HFI maps together to improve results. We are also planing to implement polarization data in this project to investigate these haze/bubble signals closely as by using only temperature maps we can not investigate all the features of this haze/bubble.

In this project we used modified "ILC (Iterative Linear Combination)" of WMAP with "Metropolis-Hasting of Markov Chain Monte Carlo" simulation and got some good satisfactory results. We used "Metropolis-Hasting of Markov Chain Monte Carlo" for sampling of all the parameters (*i.e.* spectral index of foreground components, dipole, monopole and noise). By using this approach we do get some good results but still results are not very impressive. So in future we are looking for some better sampling as well as data analysis approach like *Conditional Random Sampling (CRF)* to do better sampling of parameters. These processes decrease computation time as well as decrease computational errors.

BIBLIOGRAPHY

- [1] Spergel, D. N., Verde, L., Peiris, H. V., et al. 2003, ApJS, 148, 175
- [2] Bennett, C. L., Hill, R. S., Hinshaw, G., et al. 2003, ApJS, 148, 97
- [3] de Oliveira-Costa, A., Tegmark, M., Finkbeiner, D. P., et al. 2002, ApJ, 567, 363
- [4] Finkbeiner, D. P. 2004, ApJ, 614, 186
- [5] Dobler, G., & Finkbeiner, D. P. 2008a, ApJ, 680, 1222
- [6] Dobler, G., Finkbeiner, D. P., Cholis, I., Slatyer, T., & Weiner, N. 2010, ApJ, 717, 825
- [7] Su, M., Slatyer, T. R., & Finkbeiner, D. P. 2010, ApJ, 724, 1044
- [8] Crocker, R. M., & Aharonian, F. 2011, Phys. Rev. Lett., 106, 101102
- [9] Biermann, P. L., Becker, J. K., Caceres, G., et al. 2010, ApJ, 710, L53
- [10] Hooper, D., Finkbeiner, D. P., & Dobler, G. 2007, Phys. Rev. D, 76, 083012
- [11] Gold, B., Odegard, N., Weiland, J. L., et al. 2011, ApJS, 192, 15
- [12] Mertsch, P., & Sarkar, S. 2010, JCAP, 10, 19
- [13] Dickinson, C., Eriksen, H. K., Banday, A. J., et al. 2009, ApJ, 705, 1607
- [14] Ade, P. A. R. "Planck intermediate results. IX. Detection of the Galactic haze with Planck," A&A554 (2013) A139." arXiv preprint arXiv:1208.5483. APA

- [15] Einasto, Jaan. "Dark matter." arXiv preprint arXiv:0901.0632 (2009). APA
- [16] Allen, B., et al. "CMB Anisotropy Induced by Cosmic Strings on Angular Scales > 15'." arXiv preprint astro-ph/9704160 (1997).APA
- [17] C. L. Bennett, A. J. Banday, K. M. Gorski, G. Hinshaw, P. Jackson, P. Keegstra, A. Kogut, G. F. Smoot, D. T. Wilkinson, and E. L. Wright, ApJL, 464, L1 (1996).
- [18] G. Hinshaw, D. Larson, E. Komatsu, D. N. Spergel, C. L. Bennett, J. Dunkley, M. R. Nolta, M. Halpern, R. S. Hill, N. Odegard, L. Page, K. M. Smith, J. L. Weiland, B. Gold, N. Jarosik, A. Kogut, M. Limon, S. S. Meyer, G. S. Tucker, E. Wollack, and E. L. Wright, ApJS, 208, 19 (2013).
- [19] P. A. R. Ade et al. [Planck Collaboration], arXiv:1303.5076.
- [20] C. L. Bennett, D. Larson, J. L. Weiland, N. Jarosik, G. Hinshaw, N. Odegard, K. M. Smith, R. S. Hill, B. Gold, M. Halpern, E. Komatsu, M. R. Nolta, L. Page, D. N. Spergel, E. Wollack, J. Dunkley, A. Kogut, M. Limon, S. S. Meyer, G. S. Tucker, and E. L. Wright, ApJS, 208, 20 (2013).
- [21] B. Gold, N. Odegard, J. L. Weiland, R. S. Hill, A. Kogut, C. L. Bennett, G. Hinshaw, X. Chen, J. Dunkley, M. Halpern, N. Jarosik, E. Komatsu, D. Larson, M. Limon, S. S. Meyer, M. R. Nolta, L. Page, K. M. Smith, D. N. Spergel, G. S. Tucker, E. Wollack, and E. L. Wright, ApJS, 192, 15 (2011).
- [22] P. A. R. Ade et al. [Planck Collaboration], A&A, 536, A19 (2011).
- [23] A. de Oliveira-Costa, M. Tegmark, D. P. Finkbeiner, R. D. Davies, C. M. Gutierrez, L. M. Haffner, A. W. Jones, A. N. Lasenby, R. Rebolo, R. J. Reynolds, S. L. Tufte, and R. A. Watson, ApJ, 567, 363 (2002).
- [24] CMB foreground: A concise review, 2014PTEP.2014fB109I

-
- [25] Saha, Rajib, and Pavan K. Aluri. "A Perturbative Analysis of Synchrotron Spectral Index Variation over the Microwave Sky." *The Astrophysical Journal* 829.2 (2016): 113.APA